Further Test of Third Order + Second-Order Perturbation DFT Approach: Hard Core Repulsive Yukawa Fluid Subjected to Diverse External Fields

Shiqi Zhou*

Institute of Modern Statistical Mechanics, Zhuzhou Institute of Technology, Wenhua Road, Zhuzhou city, 412008, P. R. China

Andrej Jamnik

University of Ljubljana, Faculty of Chemistry and Chemical Technology, Aškerčeva 5, SI-1001 Ljubljana, Slovenia

Received: November 23, 2005; In Final Form: January 16, 2006

Grand canonical Monte Carlo simulation is used to investigate density profiles of hard-core repulsive Yukawa (HCRY) model fluid under the influence of various external fields and radial distribution function (RDF) of the bulk HCRY system. The aim of these extensive simulations is to provide exact data for purely repulsive interaction potential against which the validity of a third order + second-order perturbation DFT approach can be tested. It is found that a semiempirical parametrized bridge function due to Malijevsky and Labik performs very well for the RDF of the bulk HCRY fluid. Incorporation of a bulk second-order direct correlation function (DCF) of the HCRY fluid based on the Malijevsky−Labik bridge function into the third order + second-order perturbation DFT approach yields the resulting theoretical predictions for the density profiles of inhomogeneous HCRY fluid that are in a very good agreement with the simulation data, an exception being somewhat larger deviations appearing for the structure of the fluid around the center of a hard spherical cavity. Both theory and simulation predict layering transition and gas−liquid coexistence phenomena occurring with the HCRY model fluid under confined conditions. For the case of an inverse sixth-power repulsive potential under the influence of a flat stationary wall defined by an inverse twelfth-power repulsive potential, the present third order + second-order perturbation DFT approach is found to be superior to several existing weighted density approximations (WDA) and partitioned WDA.

Introduction

Structure of fluids consisting of particles interacting through hard-core repulsion plus attractive tail interactions has been extensively investigated using both the pure theories and simulation, and has been also determined experimentally.[1] Numerous theoretical treatments lead to the appearance of the density functional approximation[2] (DFA) for the excess Helmholtz free energy $F_{ex}(\rho)$ or its first-order functional derivative $C^{(1)}(\mathbf{r};\rho)$, whose combination within the framework of the density functional theory[3] (DFT) constitutes a powerful theoretical tool for the structural investigation of inhomogeneous fluids including surface phenomena. The existing DFAs[2,4,5] being proposed for the nonhard sphere fluids deal with the interaction potentials that include an attractive (tail) interaction. However, their validity for the purely repulsive interparticle potentials has been never tested. There are many strictly repulsive potentials abounding within the literature, such as the inverse power potential, core-softened potential, penetrable sphere potential, purely repulsive Coulomb potential, Gaussian core potential, hard core repulsive Yukawa (HCRY) potential, etc. All these potentials can be good representatives for the situations in some real fluids. For example, the purely repulsive Coulomb potential represents the simplest model system for charged point particles immersed in a uniform neutralizing background,[6] the Gaussian core potential is usually used to represent the entropic repulsion between (the centers of mass of) self-avoiding polymer coils dispersed in a good solvent,[7] the penetrable sphere potential is usually considered as a prototype for the interaction between micelles in a solvent,[8] the core-softened potential is employed to explain the anomalous properties of water and liquid metals under specific conditions,[9] and the HCRY model can be used to study the structure and thermodynamic properties of charged colloidal particles immersed in aqueous solution of electrolyte.[10] Taking into account the generality of the purely repulsive potentials in the modeling of real fluids and considering the fact that these potentials also display interesting phase transitions in the homogeneous (bulk) phase,[11] one can guess that these models may exhibit various interesting phenomena in inhomogeneous systems. For this reason, it is very important to ascertain whether the DFAs, that have been proven suitable for the potentials incorporating attractive (tail) interactions, can be also extended and further successfully applied to the purely repulsive potentials.

In several recent publications,[12,13] it was found that the third order + second-order perturbation DFT approach[14] is very accurate for the model potentials consisting of hard core repulsion plus attractive (tail) interactions, such as hard core attractive Yukawa (HCAY) model[12,14] and Lennard−Jones (LJ) potential[13] only in the case of high reliability of the imported bulk second-order direct correlation function (DCF). The aim of the present work is to propose simulation data for the structure of HCRY model fluid subjected to various external fields originating from the presence of various spatial constrains. These data are then employed to test the validity of the third order + second-order perturbation DFT approach for purely repulsive HCRY model.

* Corresponding author e-mail: chixiayzsq@yahoo.com.

10.1021/jp056795j CCC: $33.50
Published on Web 03/09/2006

In section 2, a description of the model system is given and the open ensemble simulation employed in the present work is briefly outlined. The third order + second-order perturbation DFT approach, with the input bulk second-order DCF obtained from the numerical solution of the Ornstein−Zernike integral equation combined with a Malijevsky−Labik bridge function, is described and numerically evaluated in section 3. The resulting DFT density profiles are compared with the simulation data. Our theoretical approach is further compared with several previously existing weighted density approximations (WDA) and with a partitioned WDA for an inverse sixth-power repulsive potential subjected to an inverse twelfth-power repulsive external potential. Finally, we discuss several problems associated with the application of the present third order + second-order DFT approach, and conclude the paper with pointing out some future research directions.

2. Models and Simulation

2.1. Models. In this work we deal with the sample HCRY intermolecular potential given by

$$\beta u(r) = \infty \quad r/\sigma < 1$$
$$= \beta\epsilon\sigma \exp[-\kappa^*(r-\sigma)/\sigma]/r \quad r/\sigma > 1 \tag{1}$$

where ϵ and σ establish the energy and length scales of the potential. κ^* is the reduced interaction range or screening parameter, β has its usual meaning, $\beta = 1/kT$, k is the Boltzmann constant, and T the absolute temperature. In the following, the reduced units are used for the temperature T, $T^* = kT/\epsilon$.

Further, we investigate several cases of the source for the external potential $\varphi_{ext}(\mathbf{r})$. Besides the single hard wall, we treat also a planar gap, i.e., the two hard walls separated by a distance H, and a spherical cavity surrounded by the spherical hard wall. The external potentials due to the presence of these spatial constrains read in turn:

$$\varphi_{ext}(z) = \infty \quad z/\sigma < 0.5$$
$$= 0 \quad 0.5 < z/\sigma \tag{2}$$

for a single hard wall,

$$\varphi_{ext}(z) = \infty \quad z/\sigma < 0.5 \text{ or } z/\sigma > H/\sigma - 0.5$$
$$= 0 \quad 0.5 < z/\sigma < H/\sigma - 0.5 \tag{3}$$

for a planar slit with two plane hard walls situated at $z = 0$ and $z = H$, respectively, and

$$\varphi_{ext}(\mathbf{r}) = \infty \quad r > R$$
$$= 0 \quad r < R \tag{4}$$

for a spherical cavity with hard spherical wall of effective radius R.

2.2. Open Ensemble Simulation. For the HCRY model of eq 1 we have carried out grand canonical ensemble monte Carlo (GCEMC) simulations at constant chemical potential μ, volume V, and temperature T. This set of independent parameters that define the thermodynamic state of the system made possible the study of equilibrium between the bulk HCRY fluid and that subjected to various external fields originating from the presence of various spatial constrains. For the latter, we have chosen in turn a hard flat interface, a planar slit consisting of two parallel perfectly smooth hard walls, and finally, a closed spherical surface mimicking a spherical cavity. The general features of the GCEMC method are described elsewhere.[15] Further, some details peculiar to this study are discussed in our previous works.[12,13] Here we only mention that the reduced excess chemical potential of the bulk fluid $\beta\mu_b^{ex}$, needed as an input parameter for the open ensemble simulation of the homogeneous phase, was approximated by the analytical expression[16]

$$\beta\mu_b^{ex} = \frac{\beta A^{ex}}{N} + \frac{\beta P}{\rho_b} + \ln\rho_b - 1 \tag{5}$$

and checked by the independent GCEMC simulations of the bulk phase. The expected bulk densities were recovered within a few percents, dependent on the particular conditions. In the eq 5, A^{ex} and P are the excess free energy and pressure of the bulk Yukawa fluid, the corresponding analytical expressions can be found in the ref 16.

3. Third Order + Second-Order Perturbation DFT Approach and Numerical Results

The third order + second-order perturbation DFT approach originates from an observation that the tail part $C_{0tail}^{(2)}(r;\rho_b \cdots)$ of the bulk second-order DCF $C_0^{(2)}(r;\rho_b \cdots)$ is only weakly dependent on the bulk density. Consequently, the tail parts of the corresponding higher order (i.e., third, fourth, fifth, etc.) bulk DCFs represent very small quantities and, as such, can be ignored. For this reason, the second-order functional perturbation expansion approximation (FPEA) is sufficient for the tail part's treatment. On the contrary, the hard-core part $C_{0hc}^{(2)}(r;\rho_b \cdots)$ of the bulk second-order DCF $C_0^{(2)}(r;\rho_b \cdots)$ shows a strong dependence on the density argument. For this reason, its treatment claims an employment of the higher-order FPEA. In our previous works,[12−14] it was found that a combination of the third-order FPEA for the hard-core part and the second-order FPEA for the tail part of the bulk DCF is very successful for both the Lennard−Jones (LJ) fluid and hard core attractive Yukawa (HCAY) fluid but only on condition of high accuracy of the imported bulk second-order DCF. Therein, the details of the third order + second-order perturbation DFT approach are described, and we refer the reader to refs 12−14. Here, we only list the final expressions that are significant for the present calculations of the structure of inhomogeneous HCRY model fluid.

The first-order DCF $C^{(1)}(\mathbf{r};[\rho] \cdots)$ for the nonuniform fluids can be constructed as follows:[12−14]

$$C^{(1)}(\mathbf{r};[\rho] \cdots) = C_0^{(1)}(\rho_b \cdots) + \int d\mathbf{r}'[\rho(\mathbf{r}') - \rho_b] C_{0hc}^{(2)}(|\mathbf{r} - \mathbf{r}'|;\rho_b \cdots) + \frac{C_{0hc}^{(1)''}(\rho_b \cdots)}{2[C_{0hc}^{(1)'}(\rho_b \cdots)]^3} \int C_{0hc}^{(2)}(\mathbf{r},\mathbf{r}'';\rho_b \cdots) \times [\int C_{0hc}^{(2)}(\mathbf{r}',\mathbf{r}'';\rho_b \cdots)(\rho(\mathbf{r}') - \rho_b) d\mathbf{r}']^2 d\mathbf{r}'' + \int d\mathbf{r}_1(\rho(\mathbf{r}_1) - \rho_b) C_{0tail}^{(2)}(|\mathbf{r} - \mathbf{r}_1|;_b \cdots) = C_0^{(1)}(\rho_b \cdots) + \int d\mathbf{r}'[\rho(\mathbf{r}') - \rho_b] C_0^{(2)}(|\mathbf{r} - \mathbf{r}'|;\rho_b \cdots) + \frac{C_{0hc}^{(1)}(\rho_b \cdots)}{2[C_{0hc}^{(1)'}(\rho_b \cdots)]^3} \int C_{0hc}^{(2)}(\mathbf{r},\mathbf{r}'';\rho_b \cdots) \times [\int C_{0hc}^{(2)}(\mathbf{r}',\mathbf{r}'';\rho_b \cdots)(\rho(\mathbf{r}') - \rho_b) d\mathbf{r}']^2 d\mathbf{r}'' \tag{6}$$

In the above equation, the third-order DCF for the bulk hard sphere fluid[17] is employed for the treatment of the hard-core part, where the coefficient

$$\frac{C_{0hc}^{(1)}(\rho_b \cdots)}{2[C_{0hc}^{(1)'}(\rho_b \cdots)]^3}$$

is used as an adjustable parameter denoted by λ. Then we finally have:

$$C^{(1)}(\mathbf{r};[\rho] \cdots) = C_0^{(1)}(\rho_b \cdots) + \int d\mathbf{r}'[\rho(\mathbf{r}') - \rho_b]C_0^{(2)}(|\mathbf{r} - \mathbf{r}'|;\rho_b \cdots) + \lambda(\rho_b \cdots) \int C_{0hc}^{(2)}(\mathbf{r},\mathbf{r}'';\rho_b \cdots)[\int C_{0hc}^{(2)}(\mathbf{r}',\mathbf{r}'';\rho_b \cdots) \times (\rho(\mathbf{r}') - \rho_b)d\mathbf{r}']^2 d\mathbf{r}'' \quad (7)$$

Combination of eq 7 with the general DFT equation for the density profile of a single component fluid,

$$\rho(\mathbf{r}) = \rho_b \exp\{-\beta\varphi_{ext}(\mathbf{r}) + C^{(1)}(\mathbf{r};[\rho] \cdots) - C_0^{(1)}(\rho_b \cdots)\} \quad (8)$$

leads to the formalism enabling the calculation of the density profile $\rho(\mathbf{r})$ of the fluid under the influence of external potential $\varphi_{ext}(\mathbf{r})$. This calculation thus incorporates two externally imported parameters, i.e., the bulk second-order DCF $C_0^{(2)}(r;\rho_b \cdots)$ and the pressure of the coexistence bulk fluid from the reservoir with which the inhomogeneous fluid under consideration is in equilibrium.

A convenient route for the determination of the bulk second-order DCF $C_0^{(2)}(r;\rho_b \cdots)$ is numerical solution of the Ornstein−Zernike (OZ) integral equation (IE),

$$h(r) - C_0^{(2)}(r;\rho_b \cdots) = \rho_b \int d\mathbf{r}_1 h(\mathbf{r}_1)C_0^{(2)}(|\mathbf{r} - \mathbf{r}_1|;\rho_b \cdots) \quad (9)$$

along with the closure relation,

$$h(r) + 1 = \exp\{-\beta u(r) + \gamma + B(r)\} \quad (10)$$

Above, $\gamma(r) = h - C_0^{(2)}(r;\rho_b \cdots)$ is the indirect correlation function, and $h(r) = g(r) - 1$ is the total correlation function with $g(r)$ being the radial distribution function (RDF). B is the so-called bridge function, which is the sum of ''bridge" or ''elementary" graphs in the diagrammatic analysis of the two-point functions. Although there exists a formal relationship between $B(r)$ and $g(r)$, it involves an infinite sum of highly connected diagrams[18] which render its utilization in practical calculation impossible. For this reason, an approximation for $B(r)$ has to be made. We tried to use various bridge function approximations, such as Percus−Yevick (PY), hypernetted chain (HNC), and Rogers−Young approximation.[18,19] All of these approximations have an essential disadvantage that cannot perform satisfactorily for the whole parameter space. For example, their performance for high bulk densities ρ_b is very poor. However, a semiempirical parametrized bridge function proposed by Malijevsky and Labik[20] performs very well for the HCRY potential for the whole range of model parameters investigated.

The numerical results for the structure of HCRY fluid in various physical situations are presented in Figures 1−8. In all cases, the value for the interaction range or screening parameter κ^* is fixed at 4. In Figure 1 we present the IE theory and GCEMC bulk RDF $g(r)$ at different bulk densities and at two reduced temperatures $T^* = 0.5$ and 0.2, respectively. The theoretical RDFs are obtained by solving the OZ integral equation in combination with the Malijevsky−Labik expression

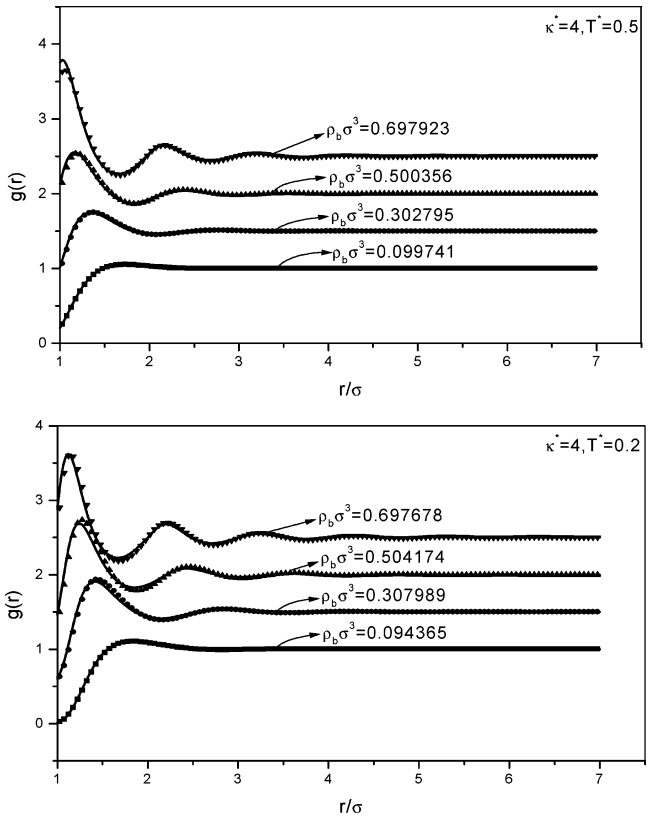

Figure 1. The theoretical (lines) and simulation (symbols) results for the bulk radial distribution function of the HCRY model fluid at two reduced temperatures and at different densities. Theoretical predictions are obtained by the use of the OZ integral equation combined with the Malijevsky−Labik bridge function. For reasons of clarity, the data corresponding to individual densities in each subfigure are shifted upward by different factors (0.5, 1,1.5, etc.).

for the bridge function. As the agreement between the results obtained by the approximate integral equation theory and simulation data is evidently very good, we can safely employ the bulk second-order DCF $C_0^{(2)}(r;\rho_b \cdots)$ based on the Malijevsky−Labik treatment of the bridge function as an input for our DFT calculation formalism.

A prerequisite condition for a validity of the present third order + second-order perturbation DFT approach is a weak density dependence of the tail part $C_{0tail}^{(2)}(r;\rho_b \cdots)$ of the bulk second-order DCF $C_0^{(2)}(r;\rho_b \cdots)$. Figure 2 shows the bulk second-order DCF as a function of the interparticle distance at different bulk densities. For the interparticle separations $r > \sigma$ we can observe very weak dependence on the density, the opposite is true for the separations $r < \sigma$. Therefore, it is natural to separate the function $C_0^{(2)}(r;\rho_b \cdots)$ into the hard-core part $C_{0hc}^{(2)}(r;\rho_b \cdots)$ and the tail part $C_{0tail}^{(2)}(r;\rho_b \cdots)$ as follows:

$$C_0^{(2)}(r;\rho_b \cdots) = C_{0hc}^{(2)}(r;\rho_b \cdots) + C_{0tail}^{(2)}(r;\rho_b \cdots) \quad (11)$$

with

$$C_{0hc}^{(2)}(r;\rho_b \cdots) = C_0^{(2)}(r;\rho_b \cdots) \quad r < \sigma$$
$$= 0 \quad r > \sigma \quad (12)$$

and

$$C_{0tail}^{(2)}(r;\rho_b \cdots) = 0 \quad r < \sigma$$
$$= C_0^{(2)}(r;\rho_b \cdots) \quad r > \sigma \quad (13)$$

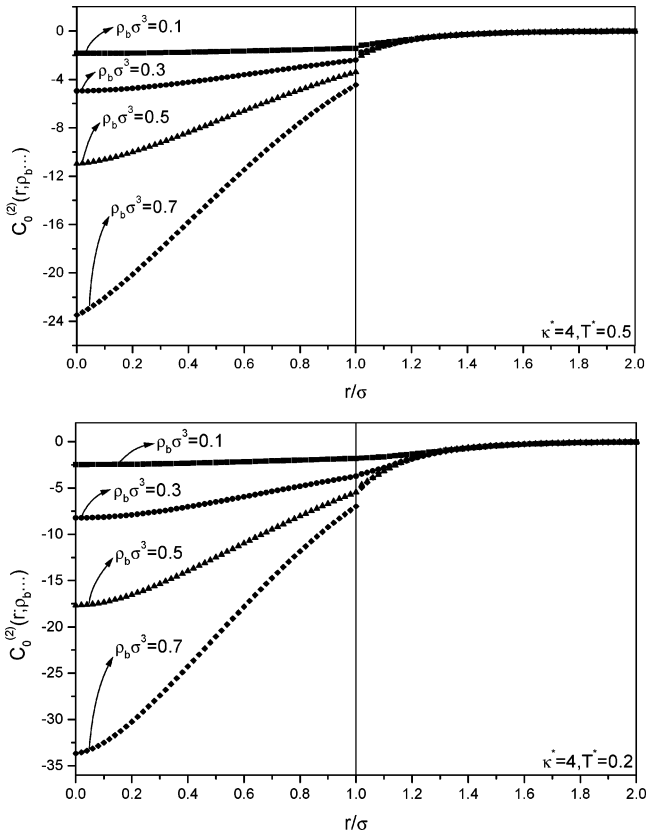

Figure 2. Bulk second-order DCF $C_0^{(2)}(r;\rho_b \cdots)$based on a combination of the OZ integral equation and Malijevsky−Labik bridge function as a function of interparticle distance at different bulk densitiesρ_b.

Determination of the adjustable parameter λ by a single hard wall sum rule similarly as done in our previous works[12−14] claims the knowledge of the pressure of the coexistence bulk fluid. To avoid small errors of the bulk pressure originating from the use of the approximate equation of state (EOS) for the HCRY fluid, which can then interfere the reliability of the judgment on the quality of the performance of the present third order + second-order perturbation DFT approach and on the expected independence of λ on the external potential responsible for the nonuniform density profile $\rho(\mathbf{r})$, we employ the exact simulation result for the pressure as an input. The pressure of the coexistence bulk fluid is thus obtained by considering the contact theorem relating the pressure and the contact density $\rho(0.5\sigma)$ and is equal to $\rho(0.5\sigma)/\beta$.

Theoretical predictions for the density profiles of HCRY fluid subjected to diverse external fields based on the present third order + second-order perturbation DFT approach and the corresponding simulation data for two sets of bulk density and potential parameters are displayed in Figures (3−8). In turn, the figures show the density profiles of the HCRY fluid: (i) at a single hard wall (Figures 3 and 4), (ii) in the planar gap of width $H = 3\sigma$ (Figures 5 and 6), and (iii) in a hard spherical cavity of effective radius $R = 3.5\sigma$ (Figures 7 and 8). The corresponding values for the adjustable parameter λ, obtained for each set of the bulk potential and density parameters, are also presented. For the sake of clarity, the majority of figures are subdivided into two or three parts, which successively illustrate the effect of increase in the bulk density at constant values of potential parameters T^* and κ^*. As reported by numerous articles in the literature dealing with the behavior of fluids at interfaces and in confined systems, a general feature found for the structure of the fluids was their spatial inhomogeneity as a consequence of the packing effects of fluid

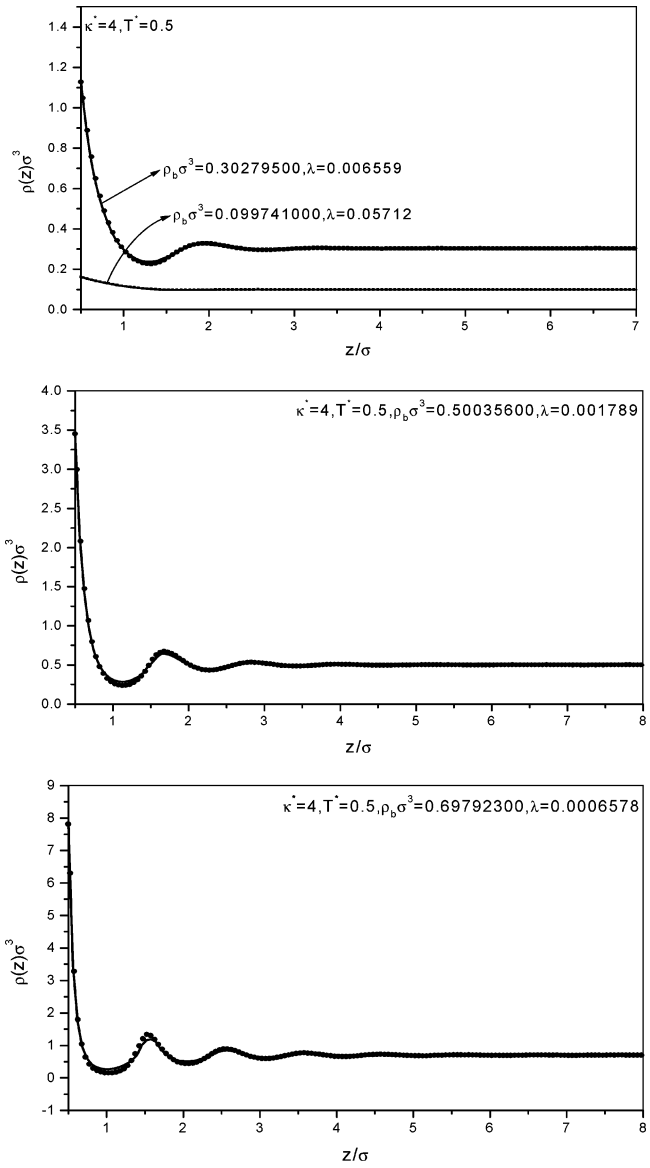

Figure 3. The theoretical (lines) and simulation (symbols) results for the density profiles of the HCRY fluid near a single hard wall at the reduced temperature $T^* = 0.5$ and at different values of the bulk density.

molecules in the domain close to the wall(s). The actual course of the density profiles, that characterize this inhomogeneity, depends on the specific nature of the fluid−fluid and the wall−fluid interactions, and on the degree and geometry of confinement. In this work as well as in our previous studies[12,13] various confined geometries have been considered in order to examine how the expressiveness of the "inhomogeneity" of the system affects the quality of the performance of DFT theory. However, the present results have an additional significance as they refer to the model fluid with purely repulsive interparticle interactions. In addition to the principal purpose of this study, i.e., the test of the DFT theory, it is also very interesting in respect of comparison of the present results with the qualitative features found for the inhomogeneous molecular models that combine both the repulsion and attraction among the molecules,[12,13] when, of course, the effect of the same spatial constraints as a source for the external potential are considered in both cases. When an inhomogeneous structure of the fluid stem from the presence of a single wall, flat density profiles $\rho(z) = \rho_b$ are restored at sufficient distances from the wall, irrespective of the specific nature of the intermolecular potential of interactions. Upon

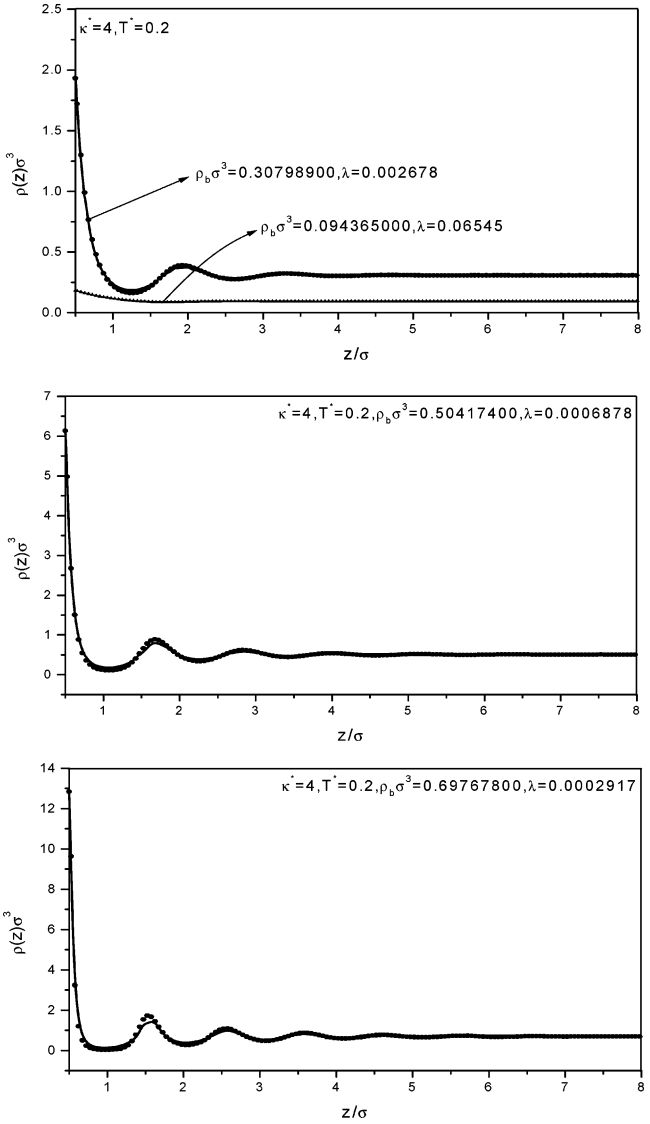

Figure 4. Same as Figure 3 but for $T^* = 0.2$.

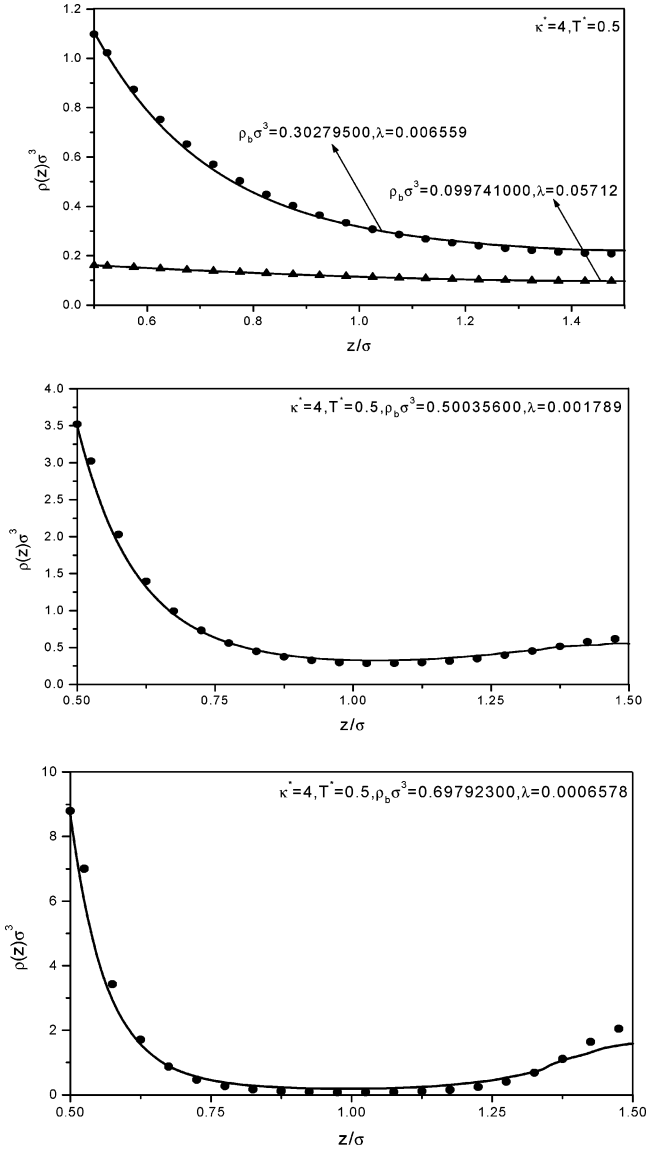

Figure 5. The theoretical (lines) and simulation (symbols) results for the density profiles of the HCRY fluid in the planar gap of width $H = 3\sigma$ at the reduced temperature $T^* = 0.5$ and at different values of the bulk density.

approaching the wall, these interactions begin to compete with steric effects. This competition, of course, is now strongly dependent on the particular intermolecular potential and in addition, on the temperature of the system. In any case, the interactions among the molecules gain in importance upon lowering temperature. As the strongly attractive molecules have a better chance for mutual attraction at sufficient distances from the wall(s) or outside the confined system, they are driven away from the hard obstacles or toward the center of the micro-objects with restricted geometry (planar gap, spherical cavity).[12,13] As expected, just the opposite behavior is observed for the molecules interacting through purely repulsive interaction potential. Clearly, strongly repulsive molecules try to avoid each other and as such they prefer the regions adjacent to the walls of the confinement. Such molecules are, therefore, accumulated next to the walls to a greater extent than those incorporating some attractive interactions thus giving rise to more pronounced packing effects leading to more distinct layering structure and higher wall−fluid contact density of the fluid with repulsive particles. As mentioned above the role of the interparticle interactions strengthens with reducing the temperature. For this reason, lowering temperature causes a decrease of the contact density and weaker oscillations in the density near the walls in the case of the model fluids with attractive molecules.[12,13] Again, just the opposite holds for the fluid of our present interest. As clearly seen from the comparisons of Figures 3 and 4 (single wall), 5 and 6 (planar gap), and 7 and 8 (spherical cavity), the contact densities (for approximately the same bulk densities) are considerably higher at the lower reduced temperature $T^* = 0.2$ (Figures 4, 6, and 8) than those at $T^* = 0.5$ (Figures 3, 5, and 7). To summarize, imposing of the qualitatively different interactions (attractive or repulsive) to the molecules of the fluid gives rise to qualitatively different redistributions of the molecules inside the confined system, leading to, thermodynamically, the most favorable structures in both cases.

A comparison of the theoretical predictions and the simulation data for the local structures of the HCRY fluid in various inhomogeneous systems indicates a very good accuracy of the present DFT theory, its actual performance being somewhat dependent on the expressiveness of the inhomogeneity of the system. For this reason, as expected, the theory does the best job in the case of a single hard wall (Figures 3 and 4) as a source of the external field, whereas slight discrepancies between the DFT and GCEMC results are observed in the case of the highest degree of confinement imposed by the presence of the

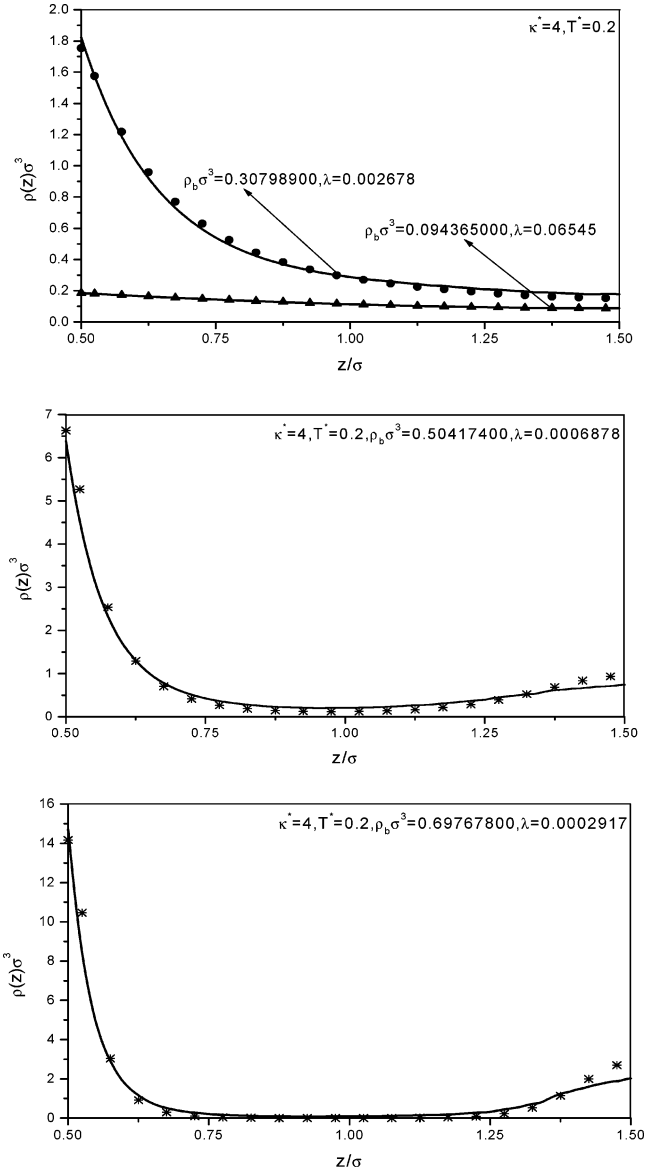

Figure 6. Same as Figure 5 but for $T^* = 0.2$.

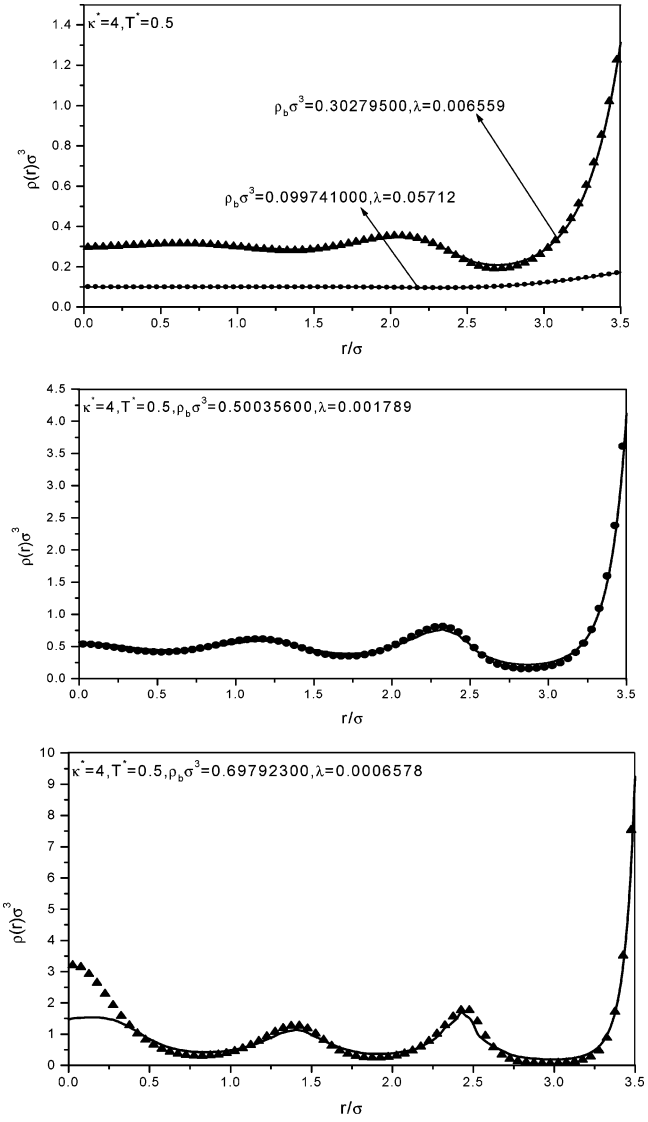

Figure 7. The theoretical (lines) and simulation (symbols) results for the density profiles of the HCRY fluid in a spherical cavity of effective radius $R = 3.5\sigma$ at the reduced temperature $T^* = 0.5$ and at different values of the bulk density.

spherical wall (Figures 7 and 8). Of course, an excellent agreement between the DFT and GCEMC density profiles near a single hard wall stem also from the fact that the adjustable parameter λ is determined by the single hard wall sum rule, where this parameter is adjusted to the value ensuring the equality of the DFT and GCEMC contact densities. Somewhat larger deviations of the DFT density from that determined by simulation can be observed in the region around the center of the spherical cavity for the highest bulk density considered (Figures 7 and 8). However, this disagreement can be ascribed to a low reliability of the simulation data for this regime stemming from a poor statistics of this part of the data. Namely, the density profile is determined from the average number of the particles found within the spherical shells into which the spherical cavity is subdivided. As the volume of these shells decreases upon approaching the center of the cavity, the counting statistics worsens in the same direction. However, since the central part is weighted by a small *r*-squared factor, even significant deviations found for the density profile in this region do not considerably affect the average density in the cavity. We can, therefore, conclude that the present theoretical approach is expected to be applicable for the study of the adsorption of the fluid in confined systems mimicking real porous materials.

It is desirable that our approach satisfactorily captures the layering transition and coexistence between the dense liquid phase and diluted gaseous phase in the confined regions.

We thus found the agreement between the simulation data and the results of the present DFT approach as, indeed, impressive. However, it is very interesting to give a further comparison between the present approach and previously existing DFAs for the same model fluid and external potentials. In ref 21, two weighted density approximations (WDAs) and a partitioned WDA are applied to the inverse sixth-power repulsive potential

$$u(r) = \epsilon\left(\frac{\sigma}{r}\right)^6 \tag{14}$$

subjected to an inverse twelfth-power repulsive external potential

$$\varphi_{ext}(r) = \epsilon\left(\frac{\sigma}{z}\right)^{12} \tag{15}$$

In Figure 9 we show the results of the present theoretical calculation for the same potential and bulk parameters as considered in ref 21, i.e., for the fixed reduced temperature

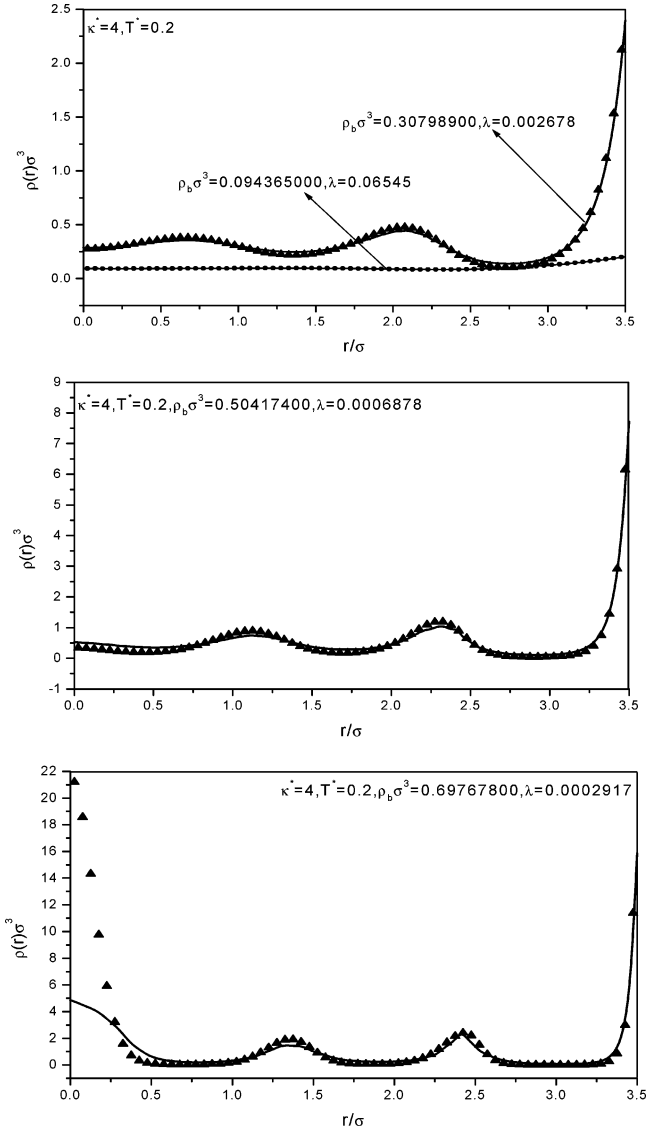

Figure 8. Same as Figure 7 but for $T^* = 0.2$.

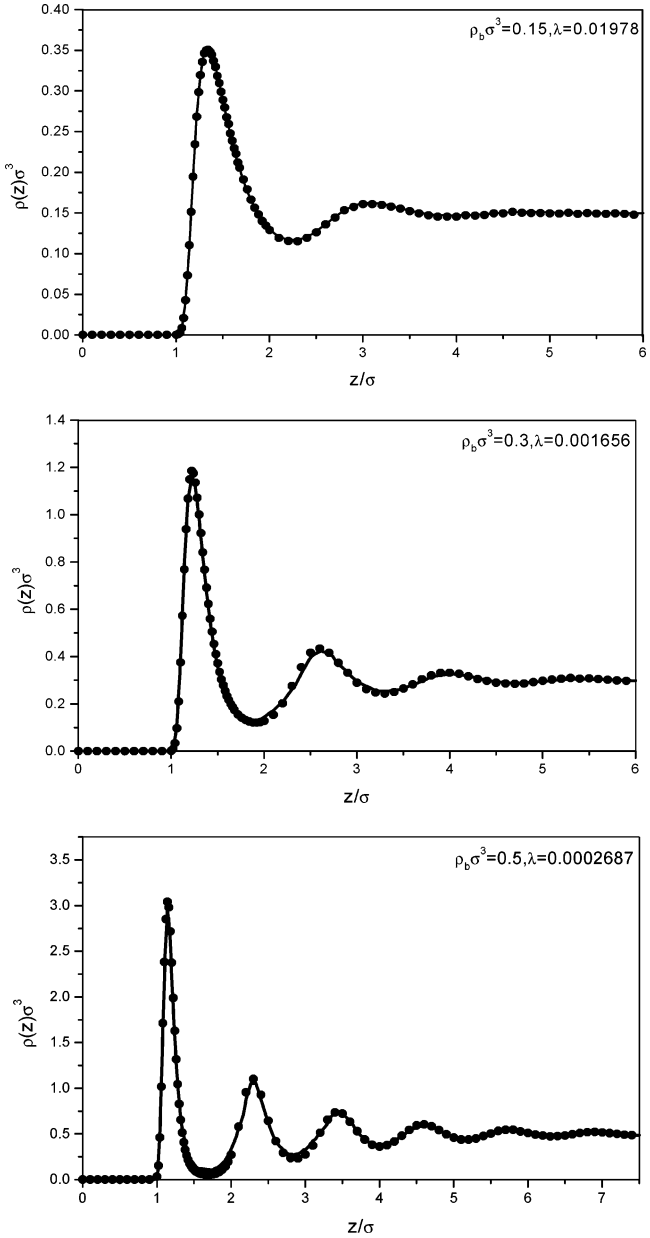

Figure 9. The theoretical (lines) and simulation (symbols) results for the density profiles of the inverse sixth-power repulsive potential fluid near a flat stationary wall defined by an inverse twelfth-power repulsive potential. The bulk and potential parameters are shown in the individual subfigures.

$T^* = 0.1$ and for three bulk densities $\rho_b\sigma^3 = 0.15$, 0.3, and 0.5. Throughout this calculation, the separating distance that appears in eqs 11−13 is σ, the bulk second-order DCF $C_0^{(2)}(r;\rho_b \cdots)$ is obtained by solving the OZ integral equation for the inverse sixth-power repulsive potential based on the RY approximation,[19] the adjustable parameter in the Rogers−Young (RY) approximation is specified by a local consistency condition, and the bulk pressure obtained via the virial route is employed to determine the parameter λ in the present third order + second-order DFT approach. Details regarding the numerical solution of the RY−OZ integral equation can be found in the article of Zhou.[22] Comparison of the results gathered in Figure 9 with those shown in Figures 1−3 of ref 21 leads to the following conclusions. The present theoretical predictions are very accurate in the case of low bulk density. Upon increasing the density, the accuracy slightly worsens but still remains higher than that found for the theoretical approaches applied in ref 21.

Although the success of the present third order + second-order perturbation DFA depends on the reliability of the input bulk second-order DCF, this observation does not devaluate it. In fact, as will be discussed in the Section 4, this dependence is inherent to all of the existing DFAs. For the van der Waals fluids, we dispose of the successful MHNC approximation[23] and hybrid mean spherical approximation HMSA,[24] which can be employed to obtain the bulk second-order DCF. For purely repulsive fluids, it is a well-known successful performance of the RY approximation,[19] which represents an interpolation between the PY and the HNC approximation. Whereas the RY approximation does not suffice for the presently investigated potential parameters for the HCRY fluid, we find out that the interpolation between other hard sphere bridge function approximations, such as BPGG approximation,[25] MS approximation[26] instead of the PY approximation, and the HNC approximation, can meet these requirements. One, therefore, does not need to worry about the unavailability of an appropriate bridge function also for other purely repulsive fluids.

4. Summary

In this paper we report extensive grand canonical Monte Carlo simulation study of the structure of the HCRY fluid subjected

to various external fields and of the structure of the same fluid in the homogeneous (bulk) phase. The HCRY fluid in the particular inhomogeneous systems maintains equilibrium with the bulk HCRY fluid. The proposed simulation data serve as a strict standard test for the validity of the present third order + second-order perturbation DFT approach. Comparison between the theoretical predictions and the simulation data leads to the conclusion that the DFT theory considered here is suitable, at least for the HCRY fluid as well as for the fluids incorporating a combination of hard core repulsion plus attractive (tail) interactions.[12−14] A prerequisite condition for a validity of this approach is a weak density dependence of the tail part of the bulk second-order direct correlation function (DCF). If this criterion is met then the overall properties of this function are governed by the stronger density dependence of its hard-core part. It would be, therefore, very important to explore the density dependence of the bulk second-order DCF for other intermolecular potentials incorporating soft repulsion, such as core-softened potential and penetrable sphere potential, and to examine whether the present third order + second-order perturbation DFT approach is applicable also to these models. Such exploration is necessary for two reasons. First, there is simply no such study published in the literature. And further, this investigation would be very interesting because of the absence of the infinite repulsive hard-core potential in these models.

The performance of DFAs, based on an approximation for the excess Helmholtz free energy, depends on the accuracy of the imported equation of state (EOS) and the bulk second-order DCF. The same holds also for the present third order + second-order perturbation DFA, which is based on the approximation for the nonuniform first-order DCF. For both kinds of DFAs, the more reliable externally imported quantities, the more accurate the DFAs' theoretical predictions. Fortunately, this dependence is continuous in both cases. In fact, it is quite gentle, which means that a small change of the value of the imported quantity, for example, that of the pressure of the coexistent bulk fluid, does not lead to a significant change of the results of DFT calculation. Correspondingly, somewhat less reliable values for the imported bulk pressure do not considerably affect the accuracy of these calculations. This statement is verified in practical calculations shown in Figure 9 where the required pressure of the equilibrium bulk fluid is taken from an approximate theory, but the accuracy of the DFT calculations remains quite satisfactory.

When applying the present third order + second-order perturbation DFA to the HCRY fluid subjected to an external field caused by a bulk HCRY particle, the resultant reduced density profile $\{\rho(r)\}/\{\rho_b\}$ is exactly the bulk radial distribution function (RDF) $g(r)$, which enables one to calculate the bulk virial pressure. By introducing the adjustable parameter λ, one can achieve the equality of the virial pressure obtained by the DFT and that following from the OZ integral equation theory (IET). For the same set of bulk potential and density parameters, the same value of λ then enters the present DFA applied for the calculation of the density profiles of the fluid under the influence of any other external field. However, the accuracy of the results for the structure of inhomogeneous fluid based on such determination of the adjustable parameter λ is obviously worse than that based on λ obtained by considering the single hard wall sum rule. There exist two explanations for this observation. The first stem from the fact that the OZ IET is only an approximate theory, thus giving rise the virial pressure obtained via this theory to yield different value for the parameter λ than that following from the exact simulation data. An inaccurate value for the DFT contact density, in the case of the single hard wall, then results in the worse performance of the DFT calculations for other external potentials. The second explanation follows the fact that the present DFT approach is itself an approximate theory. Then, even when we would retain an exact OZ IET but obtain the virial pressure by the approximate route described above, this pressure would again differ from the exact simulation value. Therefore, the origin of inaccuracy would still exist. On the basis of the above analysis, we suggest to use either the exact simulation data or an approximate EOS as an input for the DFT approach, exactly as done in the present investigation.

The presently published investigations reporting on the analysis of the reliability and applicability of the third order + second-order perturbation DFT approach are limited only to model fluids whose interaction potentials are monotonic functions of interparticle separation (plus, eventually, the hard core repulsion). However, the structural and thermodynamic properties of complex fluids are governed by an effective potential between the macroparticles, which is well-known to be an oscillatory function of the interparticle distances.[27] An especially challenging task, which remains for our future work, is, thus, the examination of the applicability of the present third order + second-order perturbation DFT approach to these effective potentials. Investigations along these lines are under progress.

Acknowledgment. The authors are pleased to acknowledge the comments from two reviewers whose suggestions were very important for the improvement of the manuscript. A.J. acknowledges the support of the Slovenian Research Agency through grant nos. P1-0201 and J1-6653. This project was also supported with the National Natural Science Foundation of China (grant no. 20546004).

References and Notes

(1) (a) Gatica, S. M.; Cole, M. W. *Phys. Rev. E.* **2005**, *72*, 041602. (b) Bohlen, H.; Schoen, M. *J. Chem. Phys.* **2004**, *120*, 6691. (c) Bonn, D.; Ross, D. *Rep. Prog, Phys.* **2001**, *64*, 1085. (d) Salamacha, L.; Patrykiejew, A.; Sokolowski, S.; Binder, K. *J. Chem. Phys.* **2005**, *122*, 074703. (e) Chialvo, A. A.; Kettler, M.; Nezbeda, I. *J. Phys. Chem. B* **2005**, *109*, 9736. (f) Zhou, S.; Jamnik, A. *Phys. Rev. E* **2006**, *73*, 011202.

(2) Henderson, D. *Fundamentals of Inhomogeneous Fluids;* Marcel Dekker: New York, 1992.

(3) Evans, R. *Adv. Phys*. **1979**, *28*, 143.

(4) (a) Quesada-Perez, M.; Martin-Molina, A.; Hidalgo-Alvarez, R. *J. Chem. Phys*. **2004**, *121*, 8618. (b) Tang, Y.; Wu, J. *Phys. Rev. E* **2004**, *70*, 011201. (c) Zhou, S.; Sun, H. *J. Phys. Chem. B* **2005**, *109*, 6397.

(5) Zhou, S. *J. Phys. Chem. B* **2004**, *108*, 3017.

(6) Baus, M.; Hansen, J. P. *Phys. Rep.* **1980**, *59*, 1.

(7) Prestipino, S.; Saija, F.; Giaquinta, P. V. *Phys. Rev. E* **2005**, *71*, 050102 (R).

(8) Marquest, C.; Witten, T. A. *J. Phys.* (France) **1989**, *50*, 1267.

(9) Skibinsky, A.; Buldyrev, S. V.; Franzese, G.; Malescio, G.; Stanley, H. E. *Phys. Rev. E* **2004**, *69*, 061206.

(10) Verwey, E. J. W.; Overbeek, J. T. G. *Theory of the Stability of Lyophobic Colloids;* Elsevier: Amsterdam, 1948.

(11) (a) Jagla, E. A. *J. Chem. Phys.* **1999**, *111*, 8980. (b) Ryzhov, V. N.; Stishov, S. M. *Phys. Rev. E* **2003**, *67*, 010201(R).

(12) Zhou, S.; Jamnik, A. *J. Chem. Phys.* **2005**, *122*, 064503.

(13) Zhou, S.; Jamnik, A. *J. Chem. Phys*. **2005**, *123*, 124708.

(14) Zhou, S. Commun. *Theor. Phys*. (Beijing, China) **2003**, *40*, 721.

(15) Frenkel, D.; Smit, B. *Understanding Molecular Simulation;* Academic Press: Boston, MA, 1996.

(16) Duh, D.; Mier-y-Teran, L. *Mol. Phys*. **1997**, *90*, 373.

(17) Zhou, S.; Ruckenstein, E. *Phys. Rev. E* **2000**, *61*, 2704.

(18) Martynov, G. A. *Fundamental Theory of Liquids. Method of Distribution Functions;* Adam Hilger: Bristol, UK, 1992.

(19) Rogers, F. J.; Young, D. A. *Phys. Rev. A* **1984**, *30*, 999.

(20) Malijevsky, A.; Labik, S. *Mol. Phys*. **1987**, *60*, 663.
(21) Sibug-Aga, R.; Laird, B. B. *Phys. Rev. E* **2004**, *69*, 051502.
(22) Zhou, S. *Can. J. Phys*. **2004**, *82*, 357.
(23) Rosenfeld, Y.; Ashcroft, N. W. *Phys. Rev. A* **1979**, *20*, 1208.
(24) Zerah, G.; Hansen, J. P. *J. Chem. Phys*. **1985**, *84*, 2336.
(25) Ballone, P.; Pastore, G.; Galli, G.; Gazillo, D. *Mol. Phys*. **1986**, *59*, 275.
(26) Martynov, G. A.; Sarkisov, G. N. *Mol. Phys*. **1983**, *49*, 1495.
(27) (a) Zhou, S. *J. Colloid Interface Sci*. **2005**, *288*, 308. (b) Zhou, S. *Chem. Phys. Lett*. **2004**, *399*, 315.